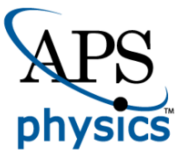

Cascaded Cavities Boost the Indistinguishability of Imperfect Quantum Emitters

Hyeongrak Choi, Di Zhu, Yoseob Yoon, and Dirk Englund

Phys. Rev. Lett. **122**, 183602 — Published 10 May 2019

DOI: 10.1103/PhysRevLett.122.183602

Cascaded Cavities Boost the Indistinguishability of Imperfect Quantum Emitters

Hyeongrak Choi[1],* Di Zhu[1], Yoseob Yoon[2], and Dirk Englund[1†]
[1]*Research Laboratory of Electronics, Massachusetts Institute of Technology, Cambridge, Massachusetts 02139, USA and*
[2]*Department of Chemistry, Massachusetts Institute of Technology, Cambridge, Massachusetts 02139, USA*
(Dated: April 10, 2019)

Recently, Grange et al. [Phys. Rev. Lett. 114, 193601 (2015)] showed the possibility of single photon generation with high indistinguishability from a quantum emitter despite strong pure dephasing, by 'funneling' emission into a photonic cavity. Here, we show that cascaded two-cavity system can further improve the photon characteristics and greatly reduce the Q-factor requirement to levels achievable with present-day technology. Our approach leverages recent advances in nanocavities with ultrasmall mode volume and does not require ultrafast excitation of the emitter. These results were obtained by numerical and closed-form analytical models with strong emitter dephasing, representing room-temperature quantum emitters.

Sources of indistinguishable single photons play an essential role in quantum information science [1], including linear-optics quantum computing [2–4], precision measurements [5], quantum simulation [6], boson sampling [7, 8], and all-optical quantum repeaters [9, 10]. Single photon sources based on atom-like quantum emitters have seen remarkable progress [11–15] including in particular color centers in diamond, many of which have been shown to possess long spin coherence times. However, a remaining challenge is to improve their emission properties to achieve near-unity indistinguishability and high collection efficiency [14, 15].

Here we show that the emission can be tailored by coupling emitter to a cascaded two-cavity system, which provides enough control to minimize detrimental effects of pure dephasing and spectral diffusion. Our analysis shows that the cascaded-cavity improves on the photon emission efficiency (η) and indistinguishability (I) compared to previously considered single-cavity approaches. For the especially difficult problem of room-temperature operation with silicon vacancy centers in diamond, the cascaded-cavity system enables same efficiency, but much higher indistinguishability (~ 0.95) than the single cavity case (~ 0.80), with $\times 20$ lower cavity quality factor (Q-factor). When the cavities are tuned for maximum ηI product, more than two orders of magnitude improvement compared to the bare emitter, and a $\sim 17\%$ improvement over the best single-cavity system are possible.

As shown in Fig. 1.(a), the linewidth of an emitter is given by $\Gamma = \gamma + \gamma^* + \Delta\delta \gg \gamma$ at room temperature, where γ is the radiative decay rate, γ^* the pure dephasing rate, and $\Delta\delta$ the FWHM width of the spectral diffusion. Pure dephasing can be modeled as Markovian phase flip process that occurs much faster than the excited-state lifetime. Whereas $\Delta\delta$ captures the spectral wandering between photoemission events (for example due to changing stray electric fields near the emitter) that changes much slower than the excited-state lifetime; thus, spectral diffusion can be treated by a statistical average over the ensemble. The indistinguishability, which is approximately given by $I \sim \gamma/\Gamma$ [18], is vanishingly small at room temperature ($\sim 10^{-4}$ for silicon vacancy centers in nanodiamond [19]).

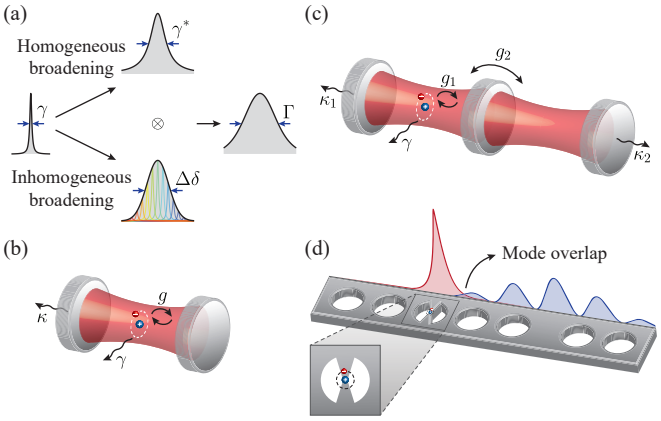

FIG. 1. (a) The emission spectrum with width Γ can be considered as a convolution of different broadenings: natural broadening (Lorentzian linewidth γ), pure dephasing (Lorentzian linewidth γ^*), and spectral diffusion (Gaussian linewidth $\Delta\delta$). (b) Cavity QED system, where g is the coupling rate, κ is the cavity decay rate, and γ is the spontaneous emission rate of the emitter to non-cavity modes. (c) Cascaded cavity system as a room temperature single photon source. An emitter is coupled to the first cavity (C_1) with coupling strength g_1. C_1 is coupled to the second cavity (C_2) with coupling strength g_2. κ_1 and κ_2 are the cavity radiation losses to free space. (d) Photonic crystal realization of the proposed cascaded-cavity-emitter system. The first cavity produces a high emitter-cavity coupling (g_1) due to the field concentration in concentric dielectric tips, see [16, 17]. A mode overlap (m.o.) of cavities corresponds to a cavity-cavity coupling rate of g_2.

Nanophotonic structures have been investigated to improve I by modifying the local density of electromagnetic states (LDOS) [20]. This approach can be analyzed in its simplest form in the cavity quantum electrodynamics (cavity-QED) picture of Fig. 1(b), where $g \propto 1/\sqrt{\mathrm{V_{eff}}}$ the emitter-cavity coupling rate, $\mathrm{V_{eff}}$ the cavity mode volume, $\kappa \propto 1/Q$ the cavity decay rate, and Q the qual-

ity factor. For simplicity, we first ignore spectral diffusion, i.e., $\Gamma = \gamma + \gamma^*$. In the incoherent regime, where the $\Gamma + \kappa \gg 2g$, the system dynamics reduces to a set of rate equations, in which the emitter and the cavity field pump each other at rate $R = 4g^2/(\Gamma + \kappa)$ [21].

There are two main approaches to increase I. One strategy is to maximize the LDOS with plasmonic cavity, so that $R = 4g^2/(\Gamma + \kappa) > \gamma^*$ [22, 23]. Peyskens et al. showed that for a 20 nm silver nanosphere ($Q \sim 15$) coupled to a waveguide, the indistinguishability of single photons emitted from SiV can be increased to $I \sim 0.27$ while reaching a single photon out-coupling efficiency of $\eta \sim 0.053$. On the other hand, Wein et al. could theoretically achieve $I \sim 0.37$ and $\eta \sim 0.77$ with the plasmonic Febry-Perot hybrid cavity ($Q \sim 986$) recently proposed in [24]. However, this approach also faces several important obstacles: (1) the assumption of instantaneous pumping on the femtoseconds scale, which is demanding due to ionization (resonant) and slow phonon relaxation (non-resonant) [25]; (2) and Ohmic and quenching losses in the metal.

A second approach investigated by Grange et al. [26] relies on coupling the emitter to a dielectric cavity with ultrahigh Q, which avoids the problems of high losses in metals. When the cavity decay rate κ is much smaller than γ and R, near-unity indistinguishability becomes possible. Notably, this system outperforms the spectral filtering of a emitted photon, due to a 'funneling' of emission into the narrow-band cavity spectrum. However, reaching an indistinguishability of 0.9 (0.5) for an emitter with $\gamma \sim 2\pi \times 100$ MHz radiative linewidth at $\omega \sim 2\pi \times 400$ THz requires a cavity with very high $Q \sim 4 \times 10^{7(6)}$; this Q far exceeds the highest quality factor nanocavity coupled to a quantum emitter, which has $Q \sim 55,000$ [27]. The underlying problem is that high indistinguishability is not possible with the limited Q and V_{eff} that are currently available.

The cascaded two-cavity system considered in this paper, illustrated in Fig. 1(c), greatly reduces the Q factor requirements while obtaining higher overall single photon source performance. The emitter is assumed to be dipole-coupled with the first cavity (C_1). This cavity can have a relatively low Q factor $< 10^5$, as long as it has a small V_{eff} to efficiently collect the emitter fluorescence. However, the indistinguishability I of the emission from cavity C_1 would be low. A high I can then be achieved by coupling to a second cavity (C_2), which provides additional degrees of freedom to optimize the single photon emission from the system.

To investigate the dynamics quantitatively, we assume a strong pure dephasing, $\gamma^* = 10^4$, normalized to $\gamma = 1$. In the regime where the total dephasing (Γ) exceeds the emitter-C_1 coupling rate g_1, the population transfer rate

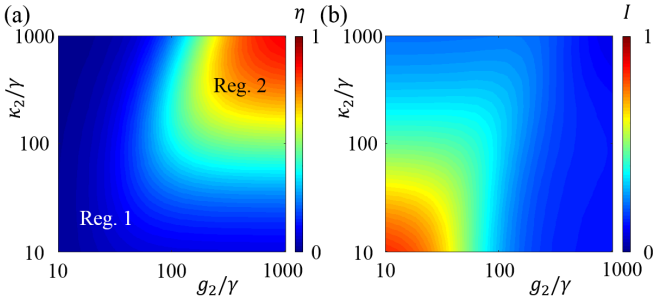

FIG. 2. Performance of the cascaded cavity system with ($g_1 = 500$, $\kappa_1 = 100$) as a function of g_2 and κ_2. Efficiency (a) and indistinguishability (b).

between the emitter and C_1 becomes [21],

$$R_1 = \frac{4g_1^2}{\Gamma + \kappa_1} \cdot \frac{1}{1 + (\frac{2\delta}{\Gamma + \kappa_1})^2}, \tag{1}$$

where δ is the detuning, assumed to be 0 for now. A large transfer rate $R_1 > \gamma$ (implying $g_1 \gg 1$) is required for efficient emission into the cavity. To this end, we make use of a new cavity design using a dielectric concentrator in a photonic crystal (PhC) nanocavity (Fig. 1(d)) [16, 17]. This nanocavity enables arbitrarily small mode volume [16]; indeed, recently $V_{\text{eff}} = 10^{-3}(\lambda/n_{\text{Si}})^3$ was experimentally demonstrated in a silicon PhC [28] with a quality factor of $\sim 10^5$. Here, we consider $g_1 = 500$ and $\kappa_1 = 50$, corresponding to $V_{\text{eff}} = 0.007(\lambda/n_{\text{diamond}})^3$ and $Q \sim 50$k for the case of silicon vacancy centers in the diamond [21, 29, 30]. In addition, the emitter is assumed to be located at the narrow bridge section of this cavity design, where the phonon environment is similar with the nanodiamond [19].

The second cavity (C_2) is coupled to C_1 at a rate g_2. This coupling can be adjusted through the spacing between the two PhC cavities, as shown in Fig. 1(d). We derived the population transfer rate between cavity C_1 and C_2 from the optical Bloch equations, by applying adiabatic elimination of the coherence between the cavities in the limit of $R_1 + \kappa_1 + \kappa_2 \gg 2g_2$ (see derivation in the Supplemental [21]). The population transfer rate between C_1 and C_2 then becomes

$$R_2 = \frac{4g_2^2}{R_1 + \kappa_1 + \kappa_2}, \tag{2}$$

where κ_2 is the decay rate of C_2. Note that if $R_1 \to 0$, R_2 reduces to the Purcell-enhanced emission rate. The R_1 term in the denominator effectively acts as additional decoherence. The reduction of the population transfer rate due to this additional decoherence was studied previously in the classical and continuous-wave (CW) limits, including for non-resonant excitation of a quantum dot [31] and for light transmission in an optomechanical system [32]. However, this decoherence directly impacts

the indistinguishability. Thus, we investigate the *temporal dynamics* of the system using master equations and non-equilibrium Green's functions.

We applied the master equation approach to calculate I and η as a function of g_2 and κ_2 for our cascaded-cavity-emitter system. The results in Fig. 2 show two regimes of interest. In 'Reg. 1' of $R_2, \kappa_2 < \kappa_1$, we find high I and small η. 'Reg. 2' of $R_2, \kappa_2 > \kappa_1$ leads to moderate I and large η. Analogous regimes were analyzed for single cavity-QED system [26]. The photon collection efficiency into C_2 follows from the Bloch equations [21] for both regimes, giving:

$$\eta = \frac{\kappa_2 R_2}{\kappa_1(\kappa_2 + R_2) + \kappa_2 R_2}. \tag{3}$$

We first focus on Reg. 1. When $R_1 \gg \kappa_1, \gamma$, the emitter and C_1 serves as a 'composite emitter' with decoherence rate R_1. This effective emitter decaying with rate $\sim \kappa_1/2$ is coupled to C_2 with $\kappa_2 < \kappa_1$ at a rate $R_2/2 < \kappa_1$ (coupling is asymmetric, and see supplemental [21] for more details). We were able to derive an analytical form for the indistinguishability with the non-equilibrium Green's function for the emitter-cavity system:

$$I = \frac{\kappa_1/2 + (\kappa_2||R_2)/2}{\kappa_1/2 + \kappa_2 + 3R_2/2}, \tag{4}$$

where $\kappa_2||R_2 = \kappa_2 R_2/(\kappa_2 + R_2)$. The same result can be derived from the quantum regression theorem [23]. Note that this equation has the similar form with the one-cavity case [26] under the substitution $(\kappa_1/2, \kappa_2, R_2/2) \to (\gamma, \kappa, R)$ — i.e., we can consider the C_1-emitter system as a 'composite emitter' inside C_2, and C_2 funnels the composite emitter as in [26]. Figure 3(a) plots η and I as a function of κ_2. Equations (3) and (4) show excellent agreement with the numerical simulations with the master equations. Notice that when $R_2 + \kappa_2 \sim R_1$, I exceeds the prediction from Eq. (4). Deviations of results from the prediction are more evident when R_1 is smaller (Fig. 3(b)). This deviation occurs because the contribution of the coherence between cavities ($\rho_{ab}(t)$) to the two-time correlation function of the cavity field, $\langle b^\dagger(t+\tau)b(t)\rangle$, is not negligible [21].

Next, we investigate Reg. 2 ($R_2, \kappa_2 > \kappa_1$), for which large η and moderate I are possible. In the C_1-emitter system with $R_1 > \kappa_1$, the excitation incoherently hops back and forth between the emitter and the cavity. Therefore, C_1 decoheres quickly at the rate R_1, resulting in a low I. On the other hand, $\kappa_1 > R_1$ also results in low I because the timing jitter of initial incoherent feeding exceeds the cavity lifetime. The solution is to choose $R_1 > \kappa_1$ and keep the population of C_1 low, preventing the photon to be re-absorbed by the emitter. C_2 provides this additional functionality with two knobs: R_2 and κ_2. When $R_2, \kappa_2 > \kappa_1$, excitation quickly passes through C_1, resulting in a low population of C_1 (P_{c1}). At the same time, the decoherence of the composite emitter (emitter-C_1) at the rate R_1 can be suppressed by a factor of $(R_1 + \kappa_1)/(R_1 + \kappa_1 + R_2||\kappa_2)$.

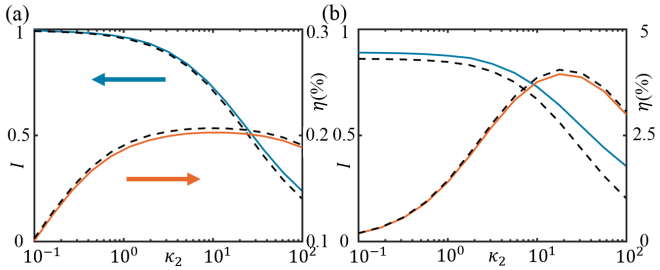

FIG. 3. High indistinguishability regime (Reg. 1). The emitter and C_1 can be treated as an effective emitter coupled to C_2 with population transfer rate $R_2/2$. (a) I (blue) and η (orange) as a function of κ_2 for $(g_1, \kappa_1, g_2) = (1500, 50, 5)$. (Solid) numerical result from master equation. (Dashed) analytical result from Eq. 4 (I) and Eq. 3 (η). (b) I and η vs. κ_2 for $(g_1, \kappa_1, g_2) = (500, 50, 10)$. The deviation between the numerical and analytical results are due to the finite effective dephasing R_1.

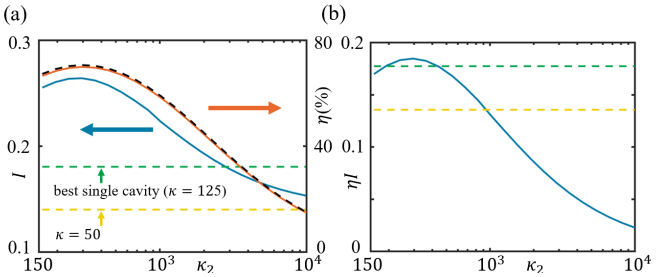

FIG. 4. Large ηI-product regime with $(g_1, \kappa_1, g_2) = (500, 50, 150)$. (a) I (blue) and η (orange) as a function of κ_2. Black dashed line is the analytical result from Eq. (3). For a single cavity system, I is plotted with yellow dashed ($g = 500$, $\kappa = 50$) and green dashed ($g = 500$, $\kappa = 125$) lines. The latter gives the maximum ηI of single cavity systems. (b) ηI-product as a function of κ_2 (blue). Cascaded cavity architecture shows higher ηI than that of single cavity system with $\kappa = 50$ (yellow dashed) and $\kappa = 125$ (green dashed, maximum ηI).

Figure 4(a) plots I and η of the photon emitted by C_2 as a function of κ_2, assuming $(g_1, \kappa_1, g_2) = (500, 50, 150)$. In the limit of large κ_2 and subsequently small R_2, the dynamics of the emitter and C_1 are the same without C_2; C_2 merely samples the photons from C_1. Thus, photons of C_2 have the same I as that of C_1 without C_2 (i.e., single-cavity system). Simulations of the single-cavity system show that photons emitted by C_1 has $I \sim 0.14$ (shown as a yellow dashed line). Decreasing κ_2 (increasing R_2) suppresses the population of C_1, increasing I. Since C_2 suffers from the same incoherent hopping/jitter effects as C_1 discussed above, I is maximized to $I = 0.27$ at $\kappa_2 = 300$. Notably, I for a $\kappa_2 = 300$ exceeds the

maximum achievable I for a single-cavity system with $g = g_1$ (green dashed line), corresponding to the same V_{eff}. Though the improvement of ηI is less significant because of a reduced efficiency (Fig. 4(b)), ηI is still higher than what single-cavity system allows.

We emphasize that in both regimes, the timing dynamics are essential in understanding the improvement of I. The Purcell enhancement (LDOS) between the emitter and C_1 barely changes due to the presence of C_2. The increase in I can be seen as a result of the modified time evolution of Green's function that governs $\langle b^\dagger(t+\tau)b(t)\rangle$ [21].

TABLE I compares the η and I values achievable for the single- and cascaded-cavity architectures, assuming a silicon vacancy center in diamond at room temperature with $(\gamma, \gamma^*, \omega) \sim (160\ \text{MHz}, 400\ \text{GHz}, 400\ \text{THz})$ [19], as a quantum emitter. To achieve I of ~ 0.95 in Reg. 1, the single-cavity approach requires a very high Q factor of 50M, which is technologically challenging, especially considering integration with the emitter. The cascaded-cavity system requires only $Q_1 = 7$k for the first cavity and $Q_2 = 500$k for the second cavity to achieve the same I. Reaching $I \sim 0.8$ requires only $Q_1 = 3.6$k and $Q_2 = 50$k for the cascaded-cavity system, whereas $Q = 10$M is needed for the single-cavity system. Note that in both cases, the cascaded cavity system also achieves much higher η values than the single-cavity case. In Reg. 2, the highest ηI is found under the constraint of $Q_{\max} = 500$ k; the cascaded-cavity system then achieves an improved $\eta I = 0.311$ ($I = 0.315$) compared to the best single-cavity system ($\eta I = 0.266$, $I = 0.267$).

Finally, we statistically incorporate inhomogeneous broadening (spectral diffusion). Figures 5(a) and 5(b) plot I and η for Reg. 1 and Reg. 2 for different $\Delta\delta$ with fixed $\gamma^* = 10^4$. We used a Gaussian probability distribution to model δ. The key observation here is that $\Delta\delta$ does not strongly diminish η and I when $\Delta\delta \ll \gamma^*$ (note that the vertical axis is highly magnified to show detail). This insensitivity to spectral diffusion follows from Eq. (1), which shows that the transfer rate (R_1) is only reduced by $\sim 2(\delta/\gamma^*)^2$, and subsequently from Eq. (2),

TABLE I. Comparison of two systems

	Cascaded-cavity I, η (%), Q_1, Q_2	Single-cavity I, η (%), Q
Reg. 1	0.950, 0.76, 7k, 500k [a]	0.950, 0.25, 50M [b]
	0.805, 3.09, 3.6k, 50k [c]	0.800, 0.27, 10M [d]
Reg. 2	0.315, 98.6, 500k, 2.1k [e]	0.267, 99.5, 3.75k [f]

[a] $g_1 = 500$, $\kappa_1 = 360$, $g_2 = 30$, $\kappa_2 = 5$
[b] $g = 1.33$, $\kappa = 0.05$
[c] $g_1 = 500$, $\kappa_1 = 700$, $g_2 = 87.5$, $\kappa_2 = 50$
[d] $g = 1.33$, $\kappa = 0.25$
[e] $g_1 = 500$, $\kappa_1 = 5$, $g_2 = 530$, $\kappa_2 = 1200$
[f] $g = 500$, $\kappa = 667$

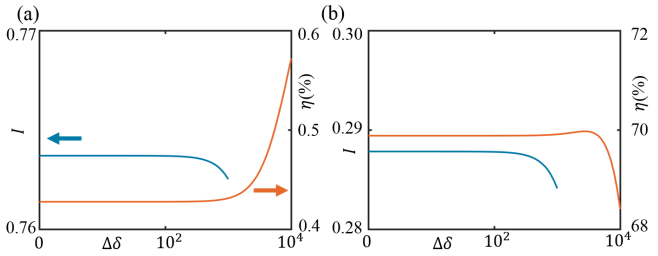

FIG. 5. I (blue) and η (red) in the presence of spectral diffusion. (a) Reg. 1 $(g_1, \kappa_1, g_2, \kappa_2)$=(500, 50, 3, 10). (b) Reg. 2 $(g_1, \kappa_1, g_2, \kappa_2)$=(500, 50, 150, 300). In both regimes, spectral diffusion marginally affects the η and I. Note that the y-axes in the figures are highly magnified to see the small change across the spectral diffusion.

that the R_2 changed by small amount. Suppression of the effect of small spectral diffusion only happens when the emitter is highly dissipative, i.e., if $\gamma + \gamma^* > \kappa$, and is a unique feature of the 'cavity funneling' process. In other words, pure dephasing serves as a resource to stabilize the single photon source, maintaining potentially high I and η despite spectral diffusion. This result is in contrast to the bare-emitter case, where the spectral diffusion directly affects I [18].

We emphasize the difference of our approach with 'photonic molecule' studied in [33, 34]. In our cascaded-cavity system, the emitter only couples with the mode of C_1, and the population is transferred between two cavity modes by weak coupling. In contrast, for the emitter coupled with a photonic molecule, the emitter is coupled to two super-modes that results from the strong coupling between two cavities, i.e., a splitting greater than the individual cavities' decay rates. Cascaded-cavity system is also different with the hybrid-cavity system [24], where the cavity mode is modified by another cavity. More specifically, in a hybrid cavity, the latter cavity field acts as a electromagnetic environment (radiation bath) of the former cavity rather than as a independent cavity mode.

In conclusion, our analysis of funneling through a cascaded-cavity revealed that it is possible to dramatically reduce the Q-factor requirements to the range of present-day feasibility. We derived closed-form analytical solutions that reproduce our numerical models. By incorporating pure dephasing and spectral diffusion, our analysis provides new insights into modification of spontaneous emission in the bad-emitter limit of cavity-QED. We also found that the cascaded cavity approach greatly improves the quality of single photons emitted from quantum emitters, promising near-unity indistinguishability even at room temperature that would be important in numerous applications such as photon-mediated entanglement [35, 36]. Applied to low-temperature emitters, we expect that it should become possible to reduce photon distinguishability to reach near-unity fidelity in photon-mediated entanglement (see supplemen-

tal [21]), which is essential for scalable quantum networks and proposed modular quantum computing architectures [37, 38].

We thank Thomas Grange, Kevin A. Fischer and Karl Berggren for helpful discussion. H.C. was supported in part by a Samsung Scholarship and the Air Force Office of Scientific Research (AFOSR) MURI on Optimal Quantum Measurements and State Verification. D.Z. was supported by the National Science Scholarship from A*STAR, Singapore. Y.Y. was supported in part by Skoltech as part of the Skoltech-MIT Next Generation Program. D.E. acknowledges partial support from the DARPA SEQUOIA program and the AFOSR PECASE program, supervised by Dr. Gernot Pomrenke.

* choihr@mit.edu
† englund@mit.edu

[1] I. Aharonovich, D. Englund, and M. Toth, Nat. Photonics **10**, 631 (2016).
[2] P. Kok, W. J. Munro, K. Nemoto, T. C. Ralph, J. P. Dowling, and G. J. Milburn, Rev. Mod. Phys **79**, 135 (2007).
[3] M. Gimeno-Segovia, P. Shadbolt, D. E. Browne, and T. Rudolph, Phys. Rev. Lett. **115**, 020502 (2015).
[4] M. Pant, D. Towsley, D. Englund, and S. Guha, arXiv:1701.03775 (2017).
[5] V. Giovannetti, S. Lloyd, and L. Maccone, Nat. Photonics **5**, 222 (2011).
[6] A. Aspuru-Guzik and P. Walther, Nat. Phys. **8**, 285 (2012).
[7] S. Aaronson and A. Arkhipov, in *Proceedings of the forty-third annual ACM symposium on Theory of computing* (ACM, 2011) pp. 333–342.
[8] J. B. Spring, B. J. Metcalf, P. C. Humphreys, W. S. Kolthammer, X.-M. Jin, M. Barbieri, A. Datta, N. Thomas-Peter, N. K. Langford, D. Kundys, *et al.*, Science , 1231692 (2012).
[9] K. Azuma, K. Tamaki, and H.-K. Lo, Nat. Commun. **6**, 6787 (2015).
[10] M. Pant, H. Krovi, D. Englund, and S. Guha, Phys. Rev. A **95**, 012304 (2017).
[11] P. Senellart, G. Solomon, and A. White, Nat. Nanotechnol. **12**, 1026 (2017).
[12] Y.-M. He, Y. He, Y.-J. Wei, D. Wu, M. Atatüre, C. Schneider, S. Höfling, M. Kamp, C.-Y. Lu, and J.-W. Pan, Nat. Nanotech. **8**, 213 (2013).
[13] N. Somaschi, V. Giesz, L. De Santis, J. Loredo, M. P. Almeida, G. Hornecker, S. L. Portalupi, T. Grange, C. Antón, J. Demory, *et al.*, Nat. Photon. **10**, 340 (2016).
[14] K. Müller, K. A. Fischer, C. Dory, T. Sarmiento, K. G. Lagoudakis, A. Rundquist, Y. A. Kelaita, and J. Vučković, Optica **3**, 931 (2016).
[15] V. Giesz, S. Portalupi, T. Grange, C. Antón, L. De Santis, J. Demory, N. Somaschi, I. Sagnes, A. Lemaître, L. Lanco, *et al.*, Phys. Rev. B **92**, 161302 (2015).
[16] H. Choi, M. Heuck, and D. Englund, Phys. Rev. Lett. **118**, 223605 (2017).
[17] S. Hu and S. M. Weiss, ACS Photonics **3**, 1647 (2016).
[18] F. W. Sun and C. W. Wong, Phys. Rev. A **79**, 013824 (2009).
[19] E. Neu, C. Hepp, M. Hauschild, S. Gsell, M. Fischer, H. Sternschulte, D. Steinmüller-Nethl, M. Schreck, and C. Becher, New J. Phys. **15**, 043005 (2013).
[20] J. Iles-Smith, D. P. McCutcheon, A. Nazir, and J. Mørk, Nat. Photon. **11**, 521 (2017).
[21] See Supplemental Material at [URL] for the master equation and optical Bloch equation of the system, adiabatic elimination and the rate equation, comparison of simulation result of master equation and rate equation, derivation of the efficiency, effective emitter method, indistinguishability of regime 1, an exemplary diamond nanocavity design, effects of small g_1, and cascaded cavity system with small dissipation and large mode volume, which includes Refs. [39–50].
[22] F. Peyskens, D. Englund, and D. Chang, Phys. Rev. B **96**, 235151 (2017).
[23] S. Wein, N. Lauk, R. Ghobadi, and C. Simon, arXiv:1710.03742 (2017).
[24] B. Gurlek, V. Sandoghdar, and D. Martín-Cano, ACS Photonics **5**, 456 (2017).
[25] N. J. Turro, V. Ramamurthy, V. Ramamurthy, and J. C. Scaiano, *Principles of molecular photochemistry: an introduction* (University Science Books, 2009).
[26] T. Grange, G. Hornecker, D. Hunger, J.-P. Poizat, J.-M. Gérard, P. Senellart, and A. Auffèves, Phys. Rev. Lett. **114**, 193601 (2015).
[27] Y. Ota, S. Iwamoto, N. Kumagai, and Y. Arakawa, Phys. Rev. Lett. **107**, 233602 (2011).
[28] S. Hu, M. Khater, R. Salas-Montiel, E. Kratschmer, S. Engelmann, W. Green, and S. Weiss, arXiv:1707.04672 (2017).
[29] A. Sipahigil, R. E. Evans, D. D. Sukachev, M. J. Burek, J. Borregaard, M. K. Bhaskar, C. T. Nguyen, J. L. Pacheco, H. A. Atikian, C. Meuwly, *et al.*, Science , aah6875 (2016).
[30] J. L. Zhang, S. Sun, M. J. Burek, C. Dory, Y.-K. Tzeng, K. A. Fischer, Y. Kelaita, K. G. Lagoudakis, M. Radulaski, Z.-X. Shen, *et al.*, Nano Lett. **18**, 1360 (2018).
[31] A. Auffèves, D. Gerace, J.-M. Gérard, M. F. m. c. Santos, L. C. Andreani, and J.-P. Poizat, Phys. Rev. B **81**, 245419 (2010).
[32] L. Fan, K. Y. Fong, M. Poot, and H. X. Tang, Nat. commun. **6**, 5850 (2015).
[33] A. Majumdar, A. Rundquist, M. Bajcsy, V. D. Dasika, S. R. Bank, and J. Vučković, Phys. Rev. B **86**, 195312 (2012).
[34] A. Majumdar, A. Rundquist, M. Bajcsy, and J. Vučković, Phys. Rev. B **86**, 045315 (2012).
[35] S. D. Barrett and P. Kok, Phys. Rev. A **71**, 060310 (2005).
[36] P. C. Humphreys, N. Kalb, J. P. Morits, R. N. Schouten, R. F. Vermeulen, D. J. Twitchen, M. Markham, and R. Hanson, Nature **558**, 268 (2018).
[37] M. Pant, H. Choi, S. Guha, and D. Englund, arXiv:1704.07292 (2017).
[38] K. Nemoto, M. Trupke, S. J. Devitt, A. M. Stephens, B. Scharfenberger, K. Buczak, T. Nöbauer, M. S. Everitt, J. Schmiedmayer, and W. J. Munro, Phys. Rev. X **4**, 031022 (2014).
[39] P. Knight and L. Allen, Phys. Rev. A **7**, 368 (1973).
[40] H. Haug and A.-P. Jauho, *Quantum kinetics in transport and optics of semiconductors*, Vol. 2 (Springer, 2008).

[41] A. Kiraz, M. Atatüre, and A. Imamoğlu, Phys. Rev. A **69**, 032305 (2004).
[42] S. Mouradian, N. H. Wan, T. Schröder, and D. Englund, Applied Physics Letters **111**, 021103 (2017).
[43] T. Iwasaki, F. Ishibashi, Y. Miyamoto, Y. Doi, S. Kobayashi, T. Miyazaki, K. Tahara, K. D. Jahnke, L. J. Rogers, B. Naydenov, *et al.*, Sci. Rep. **5**, 12882 (2015).
[44] T. Iwasaki, Y. Miyamoto, T. Taniguchi, P. Siyushev, M. H. Metsch, F. Jelezko, and M. Hatano, Phys. Rev. Lett. **119**, 253601 (2017).
[45] S. Ditalia Tchernij, T. Luhmann, T. Herzig, J. Kupper, A. Damin, S. Santonocito, M. Signorile, P. Traina, E. Moreva, F. Celegato, *et al.*, ACS Photonics **5**, 4864 (2018).
[46] R. E. Evans, M. K. Bhaskar, D. D. Sukachev, C. T. Nguyen, A. Sipahigil, M. J. Burek, B. Machielse, G. H. Zhang, A. S. Zibrov, E. Bielejec, *et al.*, Science **362**, 662 (2018).
[47] A. M. Berhane, K.-Y. Jeong, Z. Bodrog, S. Fiedler, T. Schröder, N. V. Triviño, T. Palacios, A. Gali, M. Toth, D. Englund, *et al.*, Adv. Mater. **29**, 1605092 (2017).
[48] V. A. Soltamov, A. A. Soltamova, P. G. Baranov, and I. I. Proskuryakov, Phys. Rev. Lett. **108**, 226402 (2012).
[49] T. T. Tran, K. Bray, M. J. Ford, M. Toth, and I. Aharonovich, Nat. Nanotechnol. **11**, 37 (2016).
[50] C. Chakraborty, L. Kinnischtzke, K. M. Goodfellow, R. Beams, and A. N. Vamivakas, Nat. Nanotechnol. **10**, 507 (2015).